European Rotorcraft Forum

MODAL CHARACTERISATION OF A ROTOR/PROPELLER RIG FOR TIP-MACH SCALED WIND TUNNEL TESTING

A. Tatar*, J. Wu*, D. Zagaglia†, B. Titurus*, D. Rezgui*, R.B. Green†, G. Barakos†

*: University of Bristol, Faculty of Engineering, UK

†: University of Glasgow, School of Engineering, UK

Abstract

An advanced rotor and propeller rig for tip Mach-scaled wind tunnel testing is the subject of dynamic analysis presented in this paper. Experimental modal analysis and finite element method are used to assess the key characteristics such as the modal properties and transfer functions, as well as their changes under varying conditions. This work aims to determine and summarize these characteristics for the purposes of further rig development and its safe operation. The research also includes analysis of the key sources of uncertainty, damping, the effect of unbalanced excitation and model-experiment correlation. The low frequency region is found to be dominated by the three weakly damped global modes whilst the following modes feature increased modal activity of the rotor shaft and the hub. The latter set of modes is also found to be more susceptible to nonlinear effects and associated increased identification and modelling uncertainty.

1. INTRODUCTION

The development of modern tiltrotor/tiltwing aircraft has brought the study of rotor stall and whirl flutter back to the forefront of the aerospace community [1]. In addition, with the development of modern propeller blades for acoustic efficiency, design changes may result in the alteration of the flutter boundaries. These include highly twisted and swept blades which may induce further stall towards the blade root.

Stall flutter is defined as the oscillation of the body due to a partial or full separation of the flow field around it. This was defined by Fung [2] to describe how the influence of stall flutter changes with the propeller state. Stall flutter can often be found within rotating wings, such as propellers and helicopter blades, due to the requirement of the blade to operate near the static stall angle. This can be further exacerbated with the modern thinner and highly twisted blades. Investigation on this phenomenon include the work by Ormiston et al. [3] where UH-60 flight test data was utilised to highlight some of the representative features of helicopter blade stall flutter within a pull-up manoeuvre.

To further assess this phenomenon in a more controlled laboratory environment, a novel rotor rig is being developed by the UK Vertical Lift Network (UKVLN) in the framework of the EPSRC-funded project *MENtOR* (Methods and Experiments for NOvel Rotorcraft). The UKVLN Rotor Rig is based on the National Tiltrotor Rig designed and manufactured by the Aircraft Research Association, UK [4]. The research in the MENtOR project will allow to experimentally investigate the performance of a propeller close to the stall flutter conditions. This is of importance to determine the flight envelope of tiltrotors and other aircraft that use propellers as a main source of thrust. This rig is a partial readaptation of the UK National Tiltrotor Rig [4]. The modifications have been specifically introduced to investigate the aerodynamics and aeroelasticity of a 1.2 m Mach-scaled propeller ($M_{TIP} \approx 0.6$) in flight conditions close to stall flutter, hence the need of a relatively powerful electric motor (125 kW) to meet the torque demand in that operating condition. It will be instrumented with a rotating shaft balance to measure the loads acting on the propeller, strain gauges on blades and an optical DIC (Digital Image Correlation) system to monitor the blade deformation, plus other modern flow-diagnostic techniques to investigate the propeller inflow and outflow, including Particle Image Velocimetry, Laser Doppler and hot-wire anemometry.

Due to the relatively slender nature of the upper part of the rotor rig and the presence of very heavy components at the top of the supporting structure, a modal test campaign was carried out to assess the modal characteristics and the resonances that the rig might have to cross during the spin-up and spin-down procedure. The present paper presents an analysis of the vibration properties within the frequency range related to the rig's operational properties gathered through this modal testing campaign. These results are compared with those obtained with a finite element (FE) numerical model. Finally, other possible uses of these results, such as supporting of future vibration monitoring and possible rig modifications to overcome some of the highlighted characteristics are also discussed in the paper.

Presented at 47th European Rotorcraft Forum, United Kingdom, 7-9th September, 2021

The paper is organised as follows: The modal test of the rotor rig and obtained results are introduced and analysed in Section 2. The finite element model and its comparison with the results of the modal test are presented in Section 3. The paper ends with the analysis and discussion given in Sections 3.1.

2. EXPERIMENT ANALYSIS

2.1. The rotor test rig apparatus

A schematic of the rotor rig installed inside the University of Glasgow *deHavilland* wind tunnel is presented in Figure 1. The rig sits on top of a steel framework which is bolted to the ground and connected to the turntable behind. An aluminium wing section provides support to the motor, that spins the rotor through a direct drivetrain as depicted in Figure 2. A swashplate mechanism will allow to set the cyclic and collective blade pitch angles.

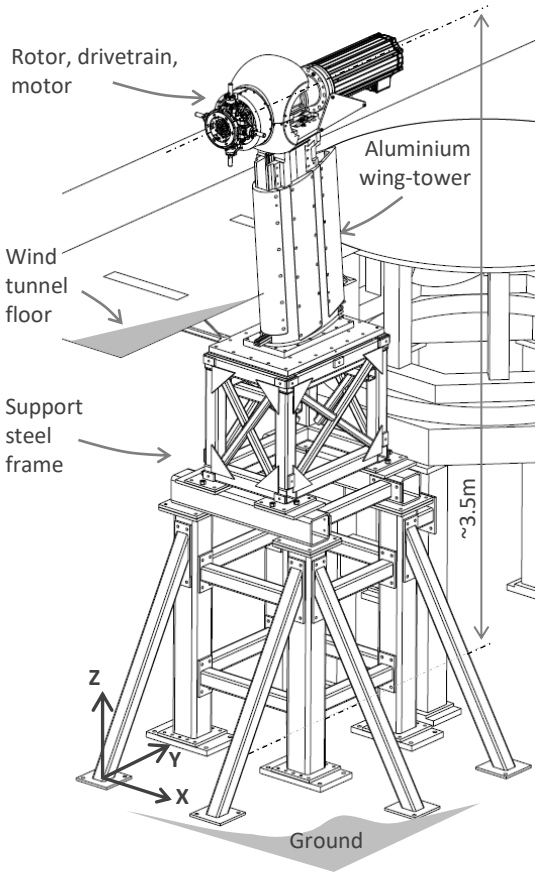

Figure 1 The rotor rig.

The centre line of the motor-drivetrain-shaft-hub assembly is positioned in the centre of the wind tunnel's working section, and the rig is free from any contact with the tunnel's floor. The steel frame part of the rig's assembly uses, predominantly, bolted fasteners and welded joints, while the top of the rig contains the complex system of bearings, pitch control mechanism, the rotor hub hinges, and other mechanical elements. It will be shown later that this composition influences a particular layout and characteristics of the identified modal properties. The investigation was conducted without the aerodynamic fairing, see Figure 2.

2.2. Experimental modal analysis

The modal tests were carried out to assess the modal properties of the resonances that the rig may have to cross during the spin-up and spin-down procedures. The present paper presents an analysis of the vibration properties within the frequency range related to the expected rig's operational characteristics gathered through this modal test campaign. These results will be compared with those obtained via a finite element (FE) numerical model.

The focus of this experimental campaign was on the modal characteristics to enable later assessment of their impact on the rotor rig performance under transient and nominal working conditions. The main objective of the experimental modal analysis (EMA) was to obtain the modal parameters of the structure [5, 6]. They were estimated in the frequency domain using the measured frequency response functions (FRFs) from the acquired acceleration responses (output) and force excitation (input). The second objective was to obtain the data suitable for validation of the FE model of the full rotor rig.

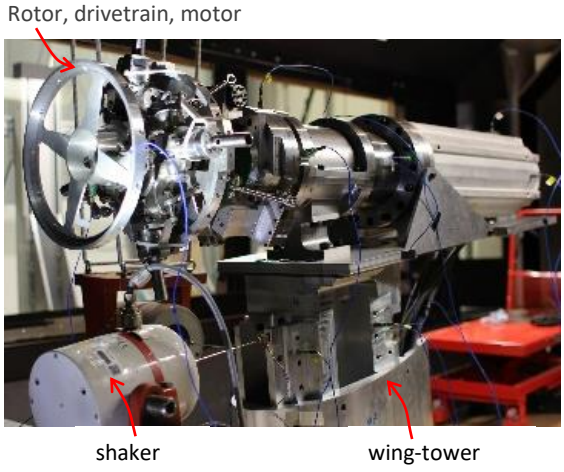

Figure 2 Detail of the top-heavy rotor rig.

EMA data acquisition for the rotor rig was conducted using *Simcenter Test Lab 18* multiple input-multiple output FRF Testing Module. The acceleration responses from the 14 measurement locations and the two force inputs were collected as shown in Figure 3. The identical single-axis ICP accelerometers (PCB 333M07) and force transducers (PCB 208C03) were used. To excite the anticipated flapwise and edgewise modes, two

electrodynamic shakers (LDS) were used, as seen in Figure 2. A summary of the main test characteristics, including the input signal and frequency response function (FRF) parameters, are presented in Table 1.

Table 1 Summary of the main test characteristics.

Test condition	*Description*
Shaker signal	Burst random between 0-1024 Hz, 90% time white noise
Input level	0.5 V, 1.0 V, 1.5 V, 2.0 V, 2.5 V
FRF parameters	Bandwidth 1024 Hz, resolution 0.0625 Hz, number of averages 8, duration 16 s

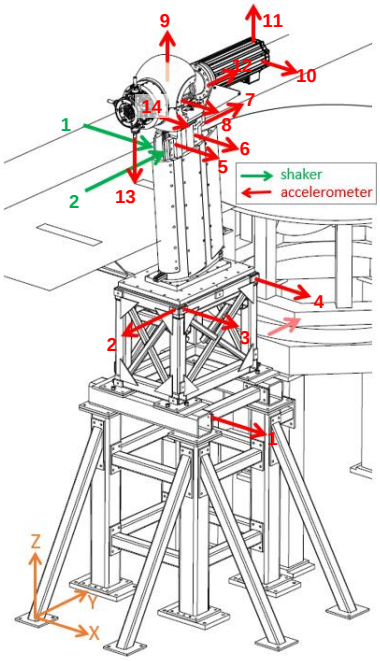

Figure 3 Locations of the accelerometers and shaker inputs used in the modal analysis tests.

The modal test was conducted several times with one or two shakers, with different excitation voltages, as well as with and without the fixing to the neighbouring turntable frame. The tests that are analysed here are summarised in Table 2.

The 14 accelerometers are placed at the positions where significant modal vibration can be generated, to allow the global mode shape to be observed. The initial (baseline) finite element model of the rotor rig provides guidance when selecting these positions. The positions of the shakers are selected to allow the major modes of the rig to be excited.

Table 2 The analysed test cases.

Test case	*Shaker ID*	*Input Voltage (V)*	*Turntable fixing?*
1	1	1.0	Yes
2	1	1.5	Yes
3	1	2.0	Yes
4	1	2.5	Yes
5	1 & 2	0.5	Yes
6 (ref.)	1 & 2	1.0	Yes
7	1 & 2	1.5	Yes
8	1	1.5	No
9	1	1.5	Yes

2.3. Modal characterization

In this section, test case 6 is used as an example and its identified modes were used to calibrate the baseline FE model. The accelerance FRFs were computed for all input-output combinations (14×2). To illustrate the frequency domain characteristics, two reference FRFs; one calculated from shaker 1 to point 5 in the flapwise (x) direction, and the other from shaker 2 to point 7 in the edgewise (y) direction, are shown in Figure 4. The FRFs are plotted for the full 1024 Hz frequency range and for the 300 Hz medium range, respectively.

The full frequency range (0-1024 Hz), Figure 4a), indicates the presence of a large number of modes. The medium frequency range, Figure 4b), highlights the significance of the “main operational frequency range” which is determined by the maximum rotor speed of the rig (3000 rpm or 50 Hz), and of the range which corresponds to the first harmonics of the blade passing frequency (BPF), i.e., 200 Hz.

For convenience of further analysis of the found modes and cross-comparison among the different test cases, the modal identification was conducted with an in-house code developed in Matlab based on the PolyMAX method [7]. The average of all identified FRFs is shown in Figure 4c) along with the modal parameter estimation results obtained from the PolyMAX method. There, the stable vibration modes were determined with the help of the stabilisation diagram (Figure 4c). The estimated modal parameters in terms of their natural frequency, damping and mode shape description are presented in Table 3.

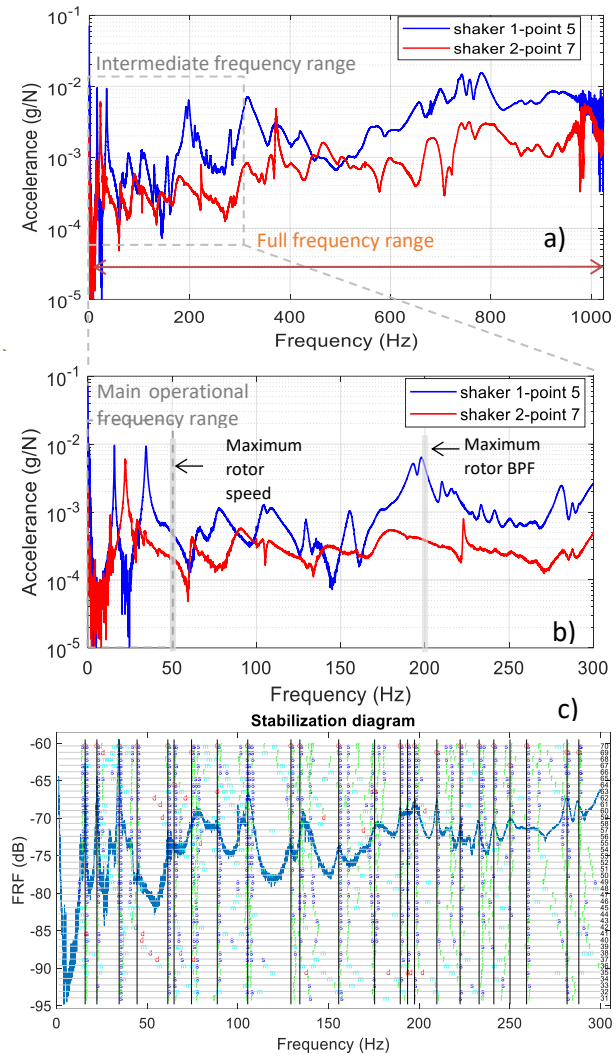

Figure 4 Rotor rig characteristics: a) the full frequency range FRFs, b) the medium frequency range FRFs, c) the stabilisation diagram by PolyMAX method.

Table 3 Summary preview of the first four identified modes from the experimental modal analysis (test case no. 6).

Mode no.	*Frequency [Hz]*	*Damping [%]*	*Mode shape description*
1 (F1)	15.73	0.77	Rig flapwise bend.
2 (L1)	22.22	1.89	Rig edgewise bend.
3 (T1)	34.49	1.14	Rig torsion
4 (S)	44.40	5.65	Shaft dominated

The mode shapes of the first four modes are illustrated in Figure 5. The first three modes of the rotor rig are global modes. The first and second modes are identified as the fundamental bending modes in the flapwise (x) and edgewise (y) directions, respectively. The third mode is identified as the torsional mode. Finally, the fourth mode is found to be associated with the localised modal activity of the shaft. These four modes are used as the reference for the following calibration of the FE model.

It can be seen that the first mode has the lowest modal damping, posing thus a particular challenge during the rig's operation in its vicinity. However, all three global modes feature relatively low damping levels highlighting the need to operate the rig at the rotor speeds which are always well separated from these critical frequencies. Compared with the first three modes, the fourth mode has a much larger damping ratio.

2.4. Frequency-damping map

In this section, to compare the results obtained from the different tests and to further scrutinize the modal characteristics of the rig, the measured test data are summarised in a frequency-damping ratio map, as shown in Figure 6. The motivation is to show how the modal properties of the rotor rig will change with the excitation level, the shaker number, and under the influence of the reinforcing connection to the turntable steel frame. Furthermore, this diagram helps with the more comprehensive and holistic understanding of the rig's dynamics across the different frequency ranges of interest, revealing different mode types and their sensitivity to the varying conditions. In this way, it can also be used to determine suitable test conditions and interpret the rig's operational characteristics arising due to effects such as the rotor unbalance excitation.

By performing modal identification for each selected test case in Table 2 using the PolyMAX method, and picking the stable poles in the stabilisation diagram (Figure 4(c)), the complete frequency-damping ratio map was generated (Figure 6). The map reveals the influence of the excitation level, the number of shakers and the absence of the additional fixing with the neighbouring steel structure on the modal properties of the rotor rig. For the first three main global modes (F1, L1 and T1), compared to the higher frequency modes, the cross-test variability among the different studied cases is relatively low.

From the distribution of the individual test points, it can be seen in Figure 6 that different types of modes respond differently to the imposed cross-test variability. In particular, the modes with the higher values of the damping ratio tend to occupy relatively localised regions, denoted here as Region 1 and Region 2, indicating thus the presence of the modes that activate a distinct dissipation mechanism which is different from the mechanism associated with the weakly damped modes. This observation is further supported by the increased sensitivity of the former modes to the increasing shaker input levels

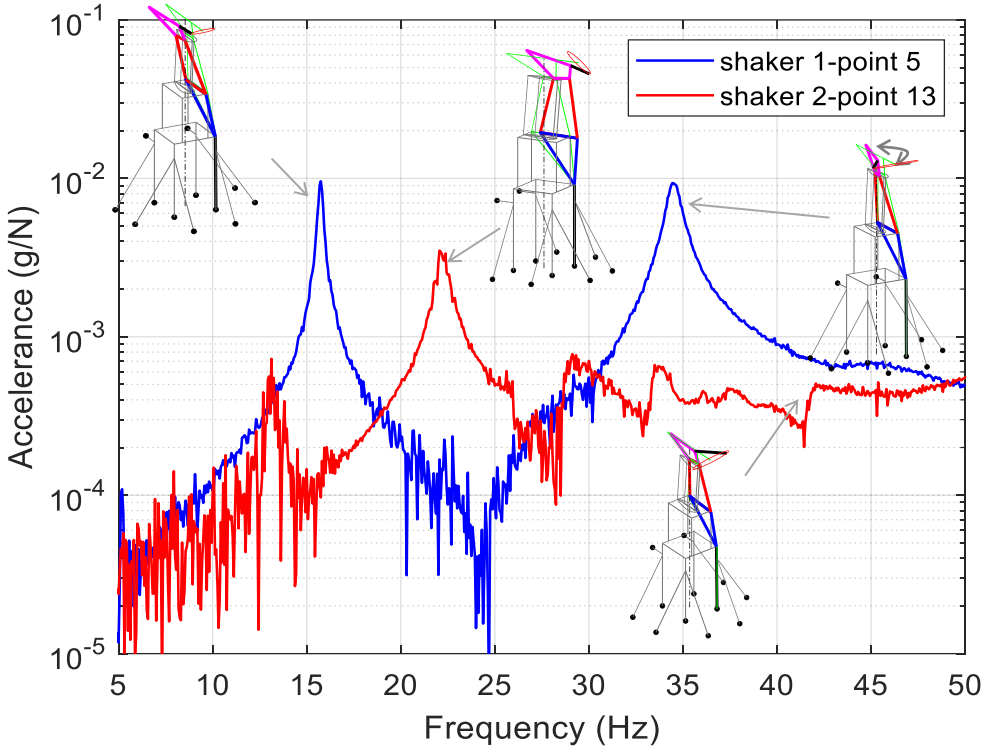

Figure 5 The reference FRFs for the main operational frequency range and the first four identified mode shapes.

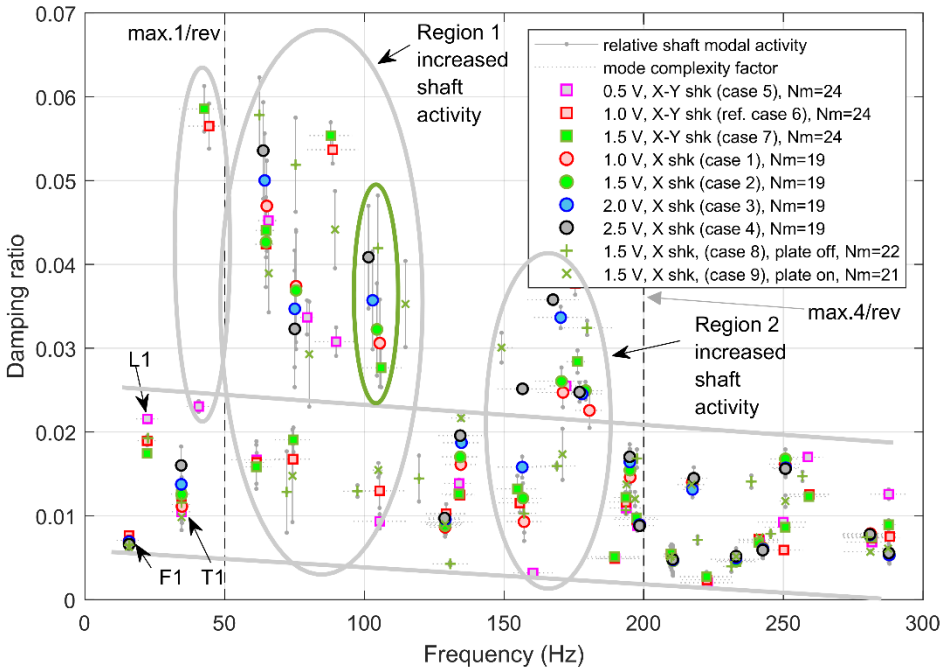

Figure 6 The frequency-damping ratio map for the nine studied test cases.

(expressed in term of the driving voltage supplied by the power amplifier in Table 2). Not only this sensitivity evidences a distinct dissipative process but, through the developed trends, it suggests the increasing engagement of the nonlinear effects. This is exemplified in the green region shown in Figure 6 where a particular mode presents itself with the decreasing natural frequency and increasing damping ratio when increasing voltage from 0.5 V to 2.5 V. Such extreme sensitivity is generally not observed in the instances of the modes with the lower damping levels. This point is further pursued by introducing additional visual information to this figure.

To convey the presence of different types of modes, each identified point is accompanied by a measure of the mode complexity (horizontal dotted grey line segments) [8] and the shaft's modal activity (vertical solid grey line segments), which is expressed as the overall motion of the rotor hub (measured coordinates 13,14) relative to the motion of the motor sub-assembly (measured coordinates 8-11). From this, high damping and damping sensitivity is typically associated with the modes with the high measure of the shaft's modal activity (e.g., see visualisation of mode 4 in Figure 5). On the other hand, the modes that retain consistently low values of damping tend to feature lower levels of the shaft's activity. The shaft's mechanical interfaces (e.g., bearings and interface with the drivetrain) are therefore seen as the sources of highly variable and increased levels of nonlinear damping. The measure of the modal complexity generally increases with the mode number and is particularly high in the modes which feature torsional motions which are not necessarily associated with the shaft's activity.

To compare the mode shapes from the modal test or between the FE model and modal test later, the modal assurance criterion (MAC) values between them are calculated. The MAC value (between 0 and 1) is used to determine the similarity of two mode shapes. The MAC value is close to 1 if two mode shapes are very close, and vice versa. The modal constants identified at the 14 positions in the modal test form a modal vector $\boldsymbol{\varphi}_{ej}$ for the j-th mode. The MAC value between these two modal vectors is calculated by

$$\mathrm{MAC}_{ij} = \frac{\left|\boldsymbol{\varphi}_{ei}^{*\mathrm{T}}\boldsymbol{\varphi}_{ej}\right|^2}{(\boldsymbol{\varphi}_{ei}^{*\mathrm{T}}\boldsymbol{\varphi}_{ei})(\boldsymbol{\varphi}_{ej}^{*\mathrm{T}}\boldsymbol{\varphi}_{ej})} \qquad (1)$$

To highlight the emergence of a group of the shaft dominated modes as well as relationships between the identified modes, the auto-MAC representation calculated using modal vectors identified from the experiment is shown in Figure 7 between the first five modes from the reference set.

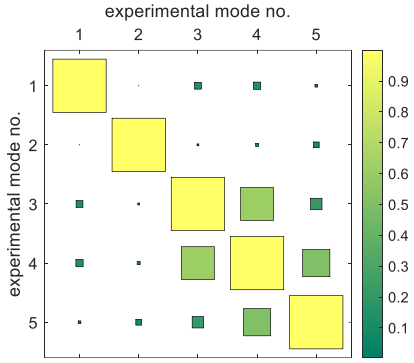

Figure 7 The auto-MAC values between the first five experimental modes.

The auto-MAC values between the experimental modes on the diagonal are all 1, and those off the diagonal are generally low, indicating that the resolution between those experimental modes is good and the chosen modal test configuration is sufficient. Figure 7 also shows that T1 (third) mode, owing to its nonnegligible shaft activity, can also be correlated against the identified mode 4. On the other hand, modes 4 and 5 demonstrate certain similarity. The results indicate the reduced identification resolution arising from the spatially localised shaft-dominated nature of the 4th and 5th modes, and more response points may need to be measured to better observe these mode shapes.

2.5. Unbalanced response study

The previous analysis is used to develop further experiment-driven picture regarding the rig's global and local dynamics and to support the following studies. Here, the focus is placed on possible resonant unbalance excitation during the run-up and run-down regimes as well as during the selected steady state test rig conditions.

The chosen measurement points and directions shown in Figure 3 enable the introduction of a measure of the steady-state rig's response due to the rotor unbalance excitation. This is achieved with the help of the reciprocity principle, applicable to the linear structural systems, by predicting the response at the locations of the shaker when the rotor rig is excited at the shaft (position 13 and 14 in Figure 3) with the use of the measured FRFs. The excitation is assumed to arise from the unbalanced rotating mass. The response at the position of shaker 1 (assuming the unbalanced mass multiplying the offset from the rotational axis as unity) is predicted as

$$U = \Omega^2 \begin{bmatrix} H_{13\to1}(\Omega) & H_{14\to1}(\Omega) \end{bmatrix} \begin{bmatrix} \mathrm{j} \\ 1 \end{bmatrix} / (\mathrm{j}\Omega)^2 \qquad (2)$$

where $H_{13\to1}$ and $H_{14\to1}$ are the FRFs from point 13 and 14 to point 1, respectively; U is the measure of

the unbalance response in the frequency domain expressed in the position of shaker 1. Due to its orientation, the inputs from the unbalanced load in directions 13 and 14 are assumed to have a phase difference of 90◦.

The responses in the frequency domain predicted for all the nine test cases were calculated and the mean and standard deviation (std) of all the nine cases were calculated at each frequency, as shown in Figure 8. They show two frequency ranges (50-100 Hz, 150-200 Hz), denoted as Region 1 and Region 2, where the variability of the response is large. These two regions are consistent with those in Figure 8, proving that the increased shaft activity and the associated nonlinear effects (e.g., due to the bearings and shaft dynamics) increase the variability of the modal frequencies and damping ratios in these two regions.

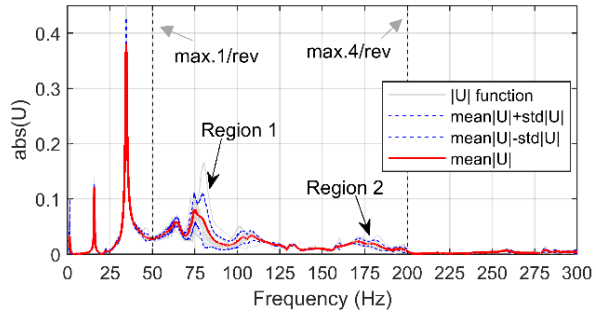

Figure 8 The flapwise rig response predicted at the position of shaker 1 due to the rotor unbalance excitation.

Figure 8 represents a useful tool to determine the safe resonance transition conditions when choosing the rotor spin-up and spin-down schedule. It can be used to select the non-resonant rotor speed test intervals characterised by the reduced vibratory environment. Further, this characteristic can be used to interpret potential operational issues associated with excessive vibrations. Such problems might arise from the higher harmonic effects due to structural (e.g., anisotropic rotor suspension) or aerodynamic asymmetries (e.g., aerodynamic shadow because of the wing-shaped tower), due to intentionally induced phenomena such as stall flutter, or due to nonlinear effects, particularly those linked with the shaft effects attributed to Region 1 and Region 2. This analysis will be beneficial in understanding how the readings of the rotating shaft balance, located at the shaft tip close to position 13 and 14, will be affected by an unbalanced loading.

3. FINITE ELEMENT ANALYSIS

To enable further analysis of the rig's dynamics, including more focused experimental data analysis, in-operation vibration monitoring planning and model-based test rig analysis of various through-life vibratory issues, an FE model was developed, tuned, and correlated against the previously discussed modal characteristics.

The medium fidelity FE model of the rig was built in Dassault Systemes SIMULIA Abaqus 2018 FE software, as seen in Figure 9. The rig was divided into three main sections: (i) the lower support, including the support frame structures, (ii) the upper support, including the frame plate and wing-shaped support tower, and (iii) the rotor assembly, including the rotor hub drivetrain, mounting plates, motor, etc. To manage the complexity of the initial pre-test FE model, a combination of the 3D beam, shell, solid, point mass and multi-point constraint elements was used.

The element types and numbers of nodes are summarised in Table 4. To model the interfaces and joints, the individual element groups and components were connected using a variety of the linking elements available including MPC Beam, Surface TIE and Structural coupling.

Table 4 Summary of the applied finite elements.

Element	*Model part*	*Nodes*
3D Solid (Hex) 3D Solid (Tet)	Wing Tower, Isolator Sheet, Motor Support, mounts, plates, etc.	91007
2D Shell (Quad)	Frame Plate	604
1D Beam	Support Frame, shafts	1397
Main rigid mass	Motor, rotor hub, swashplate, pitch links, housings, clamps, etc.	5

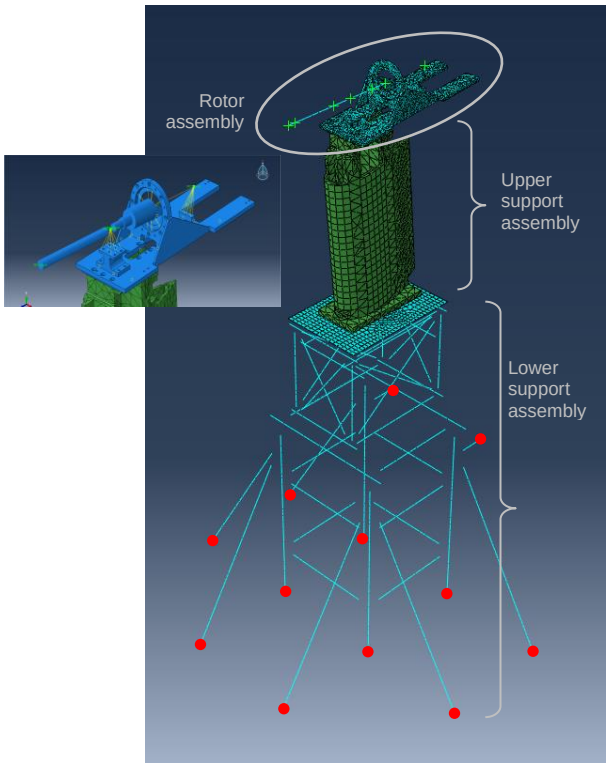

Figure 9 The finite element model of the rotor rig.

Table 5 The comparison between the FE model and experiment

FE mode no.	*Natural frequency (Hz)*		*Mode shape*	*MAC value*	*Error (%)*
	Test	*Model*			
1 (F1)	15.73	15.83	Figure 10a	0.94	0.63
2 (L1)	22.22	22.47	Figure 10b	0.74	1.12
3 (T1)	34.49	35.88	Figure 10c	0.86	4.03
5 (S)	44.40	55.30	Figure 10d	0.68	24.5

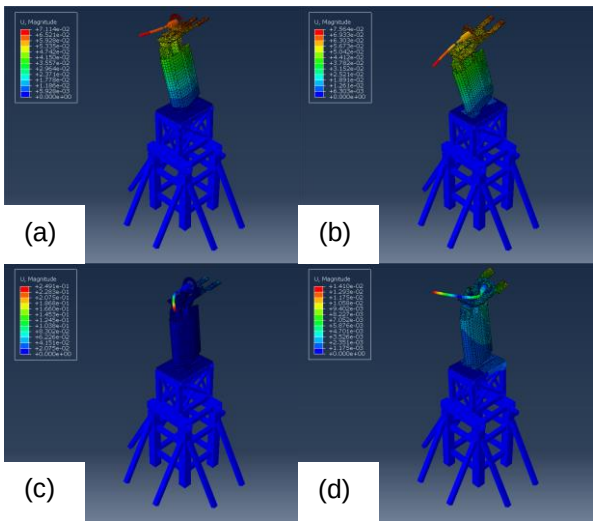

Figure 10 The mode shapes of the first three and the fifth modes calculated from the FE model

The FE model was calibrated using mainly the modal properties of the first three global modes identified in the modal test. For the primary tuning of the modal properties, first, the support frame connections, which were initially modelled using MPC tie elements, were replaced with MPC beams. This makes the overall structure slightly softer. Following, the frame plate-wing connection, which was initially modelled using Surface TIE elements, was formed by MPC beams. This enabled significant frequency reduction in the first two modes. The subsequent tuning was achieved by adjusting the drive train mass/inertia parameters, which was mostly helpful for tuning the third and fifth modes. The comparison between the FE model and experiment is made in Table 5. The modal frequencies of the FE model showed good agreement with those identified in the modal test except for the relatively large difference between the 4th experimental mode and 5th FE mode.

The first three and the fifth mode shapes calculated by the FE model are illustrated in Figure 10. To calculate the cross-MAC values with the experimental modes, the modal components for each mode at the same 14 positions as those in Figure 3 were extracted from the FE model, which formed a modal vector $\boldsymbol{\varphi}_{mi}$ for the i-th mode, and then the cross-MAC values were calculated according to Eq. (1), as shown in Figure 11.

The cross-MAC values for the first three and the fifth modes were calculated and are also listed in Table 5. The cross-MAC values for the first three global modes are high, indicating the high similarity between the mode shapes obtained from the model and identified from the experiment. The fifth mode obtained from the FE model and the fourth mode identified from the experiment are both dominated by the bending of the shaft in the horizontal plane, but the MAC value (0.68) is comparatively low. The off-diagonal cross-MAC values between the FE modes and experimental modes are small except for the 3rd FE mode and 4th experimental mode (Figure 11).

The results indicate that the FE model is not sufficiently good at representing the dynamics associated with the 4th experimental mode and needs further improvement. Such improvement is likely to be achieved by a judicious combination of the parameter tuning and increase in the FE model fidelity in the region of the pitch control mechanism. Such effort can be further enhanced by further increase of the experimental resolution in this region as indicated in Section 2.4.

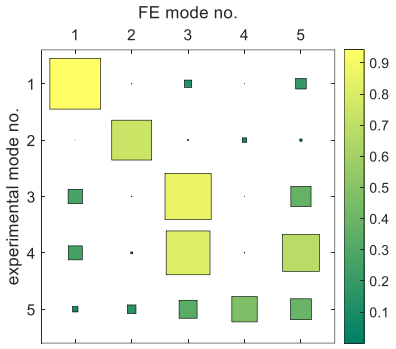

Figure 11 The cross-MAC values between the FE modes and experimental modes.

3.1. FE modelling summary

In the first and second mode, the drivetrain and shaft assembly moves with the wing assembly in-phase in the flapwise and edgewise directions, respectively. In terms of relative vibrational motion, there is only a limited elastic interaction between these assemblies in these modes. However, the elastic and other interfacial interactions are increasingly pronounced in the subsequent modes. Therefore, capturing those coupled modes accurately with the current FE model is somewhat challenging.

When calibrating the FE model, it was found that 1st and 2nd mode were particularly sensitive to the choice of the frame plate-wing assembly connection elements (MPC beams), and 3rd and 5th modes were sensitive to the drivetrain mass/inertia parameters. Initially, Surface TIE elements were chosen for the frame plate-wing assembly connection. However, the resulting global dynamic behaviour became even more rigid. Instead, MPC beam elements were used in the next step. The number and location of these MPC beams were optimised in the final analysis. This contact and interface modelling indicates that even though each part is modelled appropriately, a choice of the inaccurate connection conditions between two parts can cause significant error for the whole structure. Further, more refined tuning and modelling of the drivetrain region also increases accuracy across all considered modes in general. Specifically, the drivetrain and shaft-dominated modes such as mode 3 and 5 can be efficiently tuned with the drivetrain mass/inertia parameters.

The FE model will be helpful when planning the wind tunnel experiments. After these tests, the FE model will be further updated by considering the influence of the fairing, blades and aerodynamic effects. The resulting model will support stall flutter and other aeroelastic investigations.

Finally, noting that the first few global modes feature relatively low damping, the application of suitable passive vibration treatment can be considered, including the design of a single or multi-mode tuned vibration absorber to ensure improved operation around the current resonant frequencies in the frequency range of 0-50 Hz.

4. CONCLUSION

Experimental modal analysis was carried out on an advanced rotor and propeller rig (the UKVLN Rotor Rig), and then an extensive modal identification study was conducted using the PolyMAX method. Three global modes with relatively low modal damping ratio and one local mode with high damping were identified in the main operating frequency range (0-50 Hz). The mode shapes of these first four modes feature the global rig's flapwise bending, edgewise bending, torsion, and the local shaft-dominated activity, respectively. The identification of these vibration modes is critical for the safe rotor rig operation and handling to avoid any resonance problems, especially during the spin-up and spin-down procedures.

An FE model for the rotor rig was developed and calibrated using the modal properties of the first four modes identified in the modal test. The model shows a good agreement (relative error of less than 4.1%) with the test for both the modal frequencies and mode shapes of the first three global modes. However, the model-experiment agreement is relatively poor for the fourth experimental mode.

By extending the frequency analysis up to 300 Hz, the variability of the modal properties of the other potentially important modes was studied with the varying excitation level, number of shakers, and the existence of the fixing to the neighbouring turntable frame structure. The modal frequencies and damping showed relatively large variability in the two localized frequency regions. This variability was found to arise from the increased modal activity of the shaft and the associated nonlinearity. Finally, an experiment-based measure of the test rig's unbalance flapwise response was proposed as a tool for selection of the non-resonant test conditions.

This work will be beneficial for further rig development, its safe use in the wind tunne and the correct interpretation of the measured data, especially those coming from the rotating shaft balance.

Acknowledgement

This research is part of MENTOR (Methods and Experiments for Novel Rotorcraft) project, which is funded by the Engineering and Physical Sciences

Research Council (EPSRC) under Grant No. EP/S010378/1 and EP/S013814/1. The authors would like to acknowledge support and help of the Aircraft Research Association (ARA) throughout this research effort. BT also acknowledges useful discussion and suggestions offered by Dr Di Maio (University of Twente).

5. REFERENCE

[1] R.A. Ormiston, Revitalising advanced rotorcraft research – and the compound helicopter, The Aeronautical Journal, 120 (2016) 83-129.
[2] Y. Fung, An introduction to the theory of aeroelasticity, 1993.
[3] R. Ormiston, P. Martin, Rotor Blade Stall Flutter, Stable or Unstable? An Exploratory Investigation of NonlinearAeroelasticity, in: 63rd Annual Forum of American Helicopter Society, 2007.
[4] R.M. Morales, M.C. Turner, J. Platts, D. Pugh, A.T. McCallum, Control design of a tilting mechanism for the Uk national rotor test rig facility, in: 43rd European Rotorcraft Forum, 2017.
[5] D.J. Ewins, Modal testing: theory, practice, and application, Research Studies Press, 2000.
[6] C.R. Russell, C.W. Acree, Modal test and analysis of the NASA tiltrotor test rig, in: Proceedings of the AHS International Technical Meeting on Aeromechanics Design for Transformative Vertical Flight 2018, 2018.
[7] B. Peeters, H. Van der Auweraer, P. Guillaume, J. Leuridan, The PolyMAX frequency-domain method: a new standard for modal parameter estimation?, Shock and Vibration, 11 (2004) 395-409.
[8] P. Vacher, B. Jacquier, A. Bucharles, Extensions of the MAC criterion to complex modes, in: Proceedings of the international conference on noise and vibration engineering, 2010, pp. 2713-2726.